ACS Energy LETTERS

http://pubs.acs.org/journal/aelccp

Compatibility of Halide Bilayer Separators for All-Solid-State Batteries

Abhishek A. Panchal, Tyler N.T. Pennebaker, Elias Sebti, Yan Li, Yuheng Li, Raphaële J. Clément,* and Pieremanuele Canepa*

Cite This: *ACS Energy Lett.* 2024, 9, 5935−5944

Read Online

ACCESS | Metrics & More | Article Recommendations | Supporting Information

ABSTRACT: **Considering the lack of solid electrolytes that are electrochemically stable when in contact with a high-voltage cathode and a low-voltage metallic anode, bilayer separators in all-solid-state batteries are gaining increasing attention. However, previous studies have shown that the chemical reactivity between materials comprising the electrolyte bilayer is one of the contributing factors to the deterioration of battery performance during cycling. Here, we computationally screen the chemical compatibility of an extensive range of materials forming a bilayer separator using first-principles calculations. Notably, several bilayer separators are found to be thermodynamically stable; among them, the stability of the Li_3PO_4/Li_3InCl_6 pairing is further verified experimentally using a combination of X-ray diffraction, solid-state nuclear magnetic resonance, and X-ray photoelectron spectroscopy. This study underscores the importance of understanding the chemical compatibility of bilayer separators when engineering high-energy-density all-solid-state batteries.**

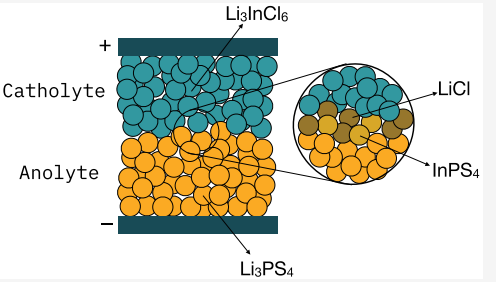

A net reduction of greenhouse gas emissions can be achieved by increasing the use of renewable energy sources, such as solar, wind, hydrothermal, and hydroelectric. However, most of these sources can supply power only intermittently and require energy storage platforms, such as rechargeable batteries, to deliver energy based on demand. Lithium-ion batteries (LIBs) are widely used as energy storage platforms in millions of portable devices. Still, LIBs have several shortcomings, preventing their increased acceptance in vehicular transportation and large infrastructure installations. For example, LIBs rely on flammable liquid organic electrolytes, which pose a safety risk.[1] The gradual increase in the energy density of commercial LIBs witnessed over the past few decades is expected to level out save for disruptive innovations in materials chemistry and device architectures.[1] One promising path toward safer LIBs is the development of all-solid-state batteries (ASSBs),[2,3] comprising nonflammable inorganic solid electrolytes (SEs). While maintaining Li-ion conductivities comparable to or better than liquid electrolytes, SEs act as physical separators; they are perceived to improve safety by compartmentalizing the high reactivity of the anode and cathode materials, preventing any leakage and reducing gassing, which is common in liquid batteries.[2] In addition, ASSBs may enable higher energy densities by replacing the graphite anode in LIBs with an energy dense Li metal anode, increasing the battery capacity and voltage.[4,5] Finally, ASSBs enable the stacking of bipolar electrodes, reducing dead weight from casing and improving the cell-level energy density.[6]

Numerous studies have focused on finding inorganic SEs enabling fast Li-ion transport (on the order of mS cm^{-1}), with oxygen-, sulfur-, phosphorus, halogen-containing materials among the most widely explored SEs. Sulfide and thiophosphate SEs show high mechanical deformability, allowing for their implementation in ASSBs via cold-pressing processes.[2,7−9] However, sulfides and thiophosphates exhibit poor oxidative (anodic) stability, reacting with high-voltage layered oxide positive electrode materials.[10−12] Oxygen-based SEs, including phosphates, exhibit wider electrochemical stability windows than sulfide SEs.[10,11] However, achieving sufficient Li-ion conductivities in oxides requires dense pellets obtained through energy intensive sintering processes, which are difficult to scale.[2,13] Additionally, the ionic conductivity of oxide SEs is typically lower than that of sulfide SEs.[7−9] Finally, ternary halide SEs with the formula Li_iMX_j (X = F, Cl, Br; *i* and *j* are determined by the oxidation state of metal M) display high electrochemical oxidative stabilities (>4 V vs Li/Li^+)[14−18] but remain unstable against Li metal.[19]

Received: September 19, 2024
Revised: November 7, 2024
Accepted: November 14, 2024

Downloaded via HONG KONG UNIV SCI TECH GUANGZHOU on December 4, 2024 at 10:53:18 (UTC).
See https://pubs.acs.org/sharingguidelines for options on how to legitimately share published articles.

© XXXX American Chemical Society

https://doi.org/10.1021/acsenergylett.4c02590
ACS Energy Lett. 2024, 9, 5935−5944

From this analysis, it is evident that none of the SEs mentioned above can simultaneously provide adequate ionic conductivity and good chemical and electrochemical stability against the electrodes, as required to achieve viable ASSBs.[10,11,20,21] The inherent reactivity results in the formation of undesired decomposition products at the electrode/SE interfaces, creating additional interfaces and increasing the interfacial (contact) resistance for Li-ion conduction, with detrimental effects on battery performance.[12,20,22]

One practical strategy to solve this issue is to combine two SEs with different chemical and electrochemical stabilities to form bilayer composite separators.[12,23−25] In these composites, the anolyte is the SE in direct contact with the low-voltage negative electrode material (e.g., graphite or Li metal and its alloys), and the catholyte is the SE in contact with the high-voltage (typically, a layered oxide) positive electrode material.

Based on their electrochemical properties, sulfide, thiophosphate, oxide, and phosphate SEs are best employed as anolytes, whereas ternary halide SEs are well suited for catholyte applications. Several studies have claimed improved electrochemical performance of ASSBs using bilayer separators: Li_6PS_5Cl/Li_3InCl_6,[19,26−29] Li_6PS_5Cl/Li_3YCl_6,[24,30,31] Li_6PS_5Cl/Li_2ZrCl_6,[32−34] $Li_{10}GeP_2S_{12}/Li_3InCl_6$,[17,35] and LGPS/$Li_2ZrCl_6$.[36] However, other investigations on similar bilayer-based ASSBs have reported battery performance degradation enabled by specific SE pairings, such as Li_6PS_5Cl/Li_3InCl_6,[12,31,37−42] Li_6PS_5Cl/Li_3YCl_6,[39] Li_6PS_5Cl/Li_2ZrCl_6,[31] and Li_3PS_4/Li_3InCl_6.[37] This degradation has been linked to the chemical incompatibility of specific anolyte and catholyte combinations with the formation of interfacial decomposition products. From these studies emerges the need to identify chemically compatible SEs to form stable and practical bilayer separators.

Screening with first-principles calculations, we analyze the thermodynamic chemical compatibility of an extensive range of inorganic materials, including oxygen- and sulfur-based SEs as anolytes and ternary halide SEs (chlorides and fluorides) as catholytes, for their potential use as bilayer separators in ASSBs. Lithium ternary fluorides were considered, as they may enhance the oxidation stability of solid electrolytes compared to their chloride analogues.[43,44] We find that the thiophosphate Li_3PS_4 and the phosphate Li_3PO_4 are the least reactive anolytes when in contact with halide catholytes. We identify a few bilayer interfaces that are thermodynamically stable upon contact. The Li_3PO_4/Li_3InCl_6 combination is examined experimentally for these few SE pairings that are predicted to be stable. Results from solid-state nuclear magnetic resonance (ssNMR), X-ray diffraction (XRD), X-ray photoelectron spectroscopy (XPS), and Raman spectroscopy suggest the excellent chemical compatibility of the Li_3PO_4/Li_3InCl_6 bilayer.

In this letter, we investigate two types of bilayer separators: sulfide/halide and oxide/halide combinations. For the sake of readability of this letter, we have included thiophosphate species, such as Li_3PS_4, Li_6PS_5Cl, and $Li_{10}GeP_2S_{12}$ in the group of sulfides, whereas Li_3PO_4 is included in the oxides. This broader classification is then avoided when discussing the specific properties of each material. Ternary halides with the formula Li_iMX_j (with X = Cl and F) are always intended as the catholyte material. Table 1 shows the possible combinations of anolytes and catholytes in this study, totaling 72 distinct bilayer interfaces.

Table 1. Materials Used as Catholytes and Anolytes in This Analysis[a]

catholytes	anolytes
chlorides: Li_2ZrCl_6, Li_3InCl_6, Li_2ZnCl_4, Li_3YCl_6, and $LiAlCl_4$	oxides: Li_2O, Li_3PO_4, and $Li_7La_3Zr_2O_{12}$
fluorides: Li_2ZrF_6, Li_3InF_6, $LiYF_4$, and Li_3AlF_6	sulfides: Li_2S, Li_3P,[b] Li_3PS_4, Li_6PS_5Cl, and $Li_{10}GeP_2S_{12}$

[a]Starting from this list, all possible combinations of anolyte/catholyte are explored. Thiophosphate and phosphate anolytes have been conveniently grouped into sulfides and oxides, respectively. [b]Li_3P is included in the sulfide SEs.

To efficiently survey the ample compositional space covered by the material combinations of Table 1, we use first-principles calculations, based on density functional theory (DFT), to probe their thermodynamic stability upon contact, often referred to as "chemical stability".[45] Knowledge of the interfacial phase diagrams enables us to identify the relevant degradation reactions that may occur upon contact between anolytes and catholytes. For example, to investigate the chemical stability of Li_3PS_4 (anolyte) with Li_3InCl_6 (catholyte), we evaluated the Li−P−S−Cl−In quinary phase diagram. Using DFT, we computed the stability of all elements and binary, ternary, quaternary, and unknown quinary compounds within this phase field at ambient temperature and pressure.

Unless explicitly mentioned, we report the predicted chemical reactions and their enthalpies after implementing two thermodynamic corrections to the DFT data. The first correction deals with the computed formation energies (FEs) of oxygen- and sulfur-containing compounds, affected by the significant systematic overbinding error for sulfur and oxygen molecules introduced by the generalized gradient approximation (GGA).[46] The second thermodynamic correction aligns the computed FEs with the experimental formation energies reported in the literature.[47] The chemical formulas of these compounds and their experimental formation energies are listed in Table S6. Reactions and enthalpies incorporating only the first correction are presented in Tables S3 and S4.

In this extended search, we consider compounds from the Inorganic Crystal Structure Database (ICSD),[48] a set augmented by hypothetical phases from the Materials Project database[49] with metastability equal to or less than 30 meV/atom above the stability line (convex hull). For hypothetical compounds, we discard structures where volume changes exceed 20% upon DFT relaxation. Whenever possible, we consider polymorphs of compounds closely matching the structures reported in the ICSD as thermodynamically stable phases. The procedure to identify all possible decomposition reactions and their enthalpies is described in detail in Section S1.

The chemical stability of an interface is determined by evaluating the "spontaneity" of the reaction triggered upon contact with the anolyte and catholyte materials. Equation 1 defines the decomposition reaction, forming n decomposition products based on a given anolyte/catholyte pair. This reaction is accompanied by a reaction enthalpy ΔH in kJ mol^{-1} (implying one mole of total reactants). Thus, the spontaneity of eq 1 is entirely determined by the change in Gibbs free energy, which is approximated in the rest of this letter by ΔH. Thus, a decomposition reaction is spontaneous when $\Delta H < 0$, and the more negative the value of ΔH, the greater the thermodynamic driving force for decomposition. We moni-

https://doi.org/10.1021/acsenergylett.4c02590
ACS Energy Lett. 2024, 9, 5935−5944

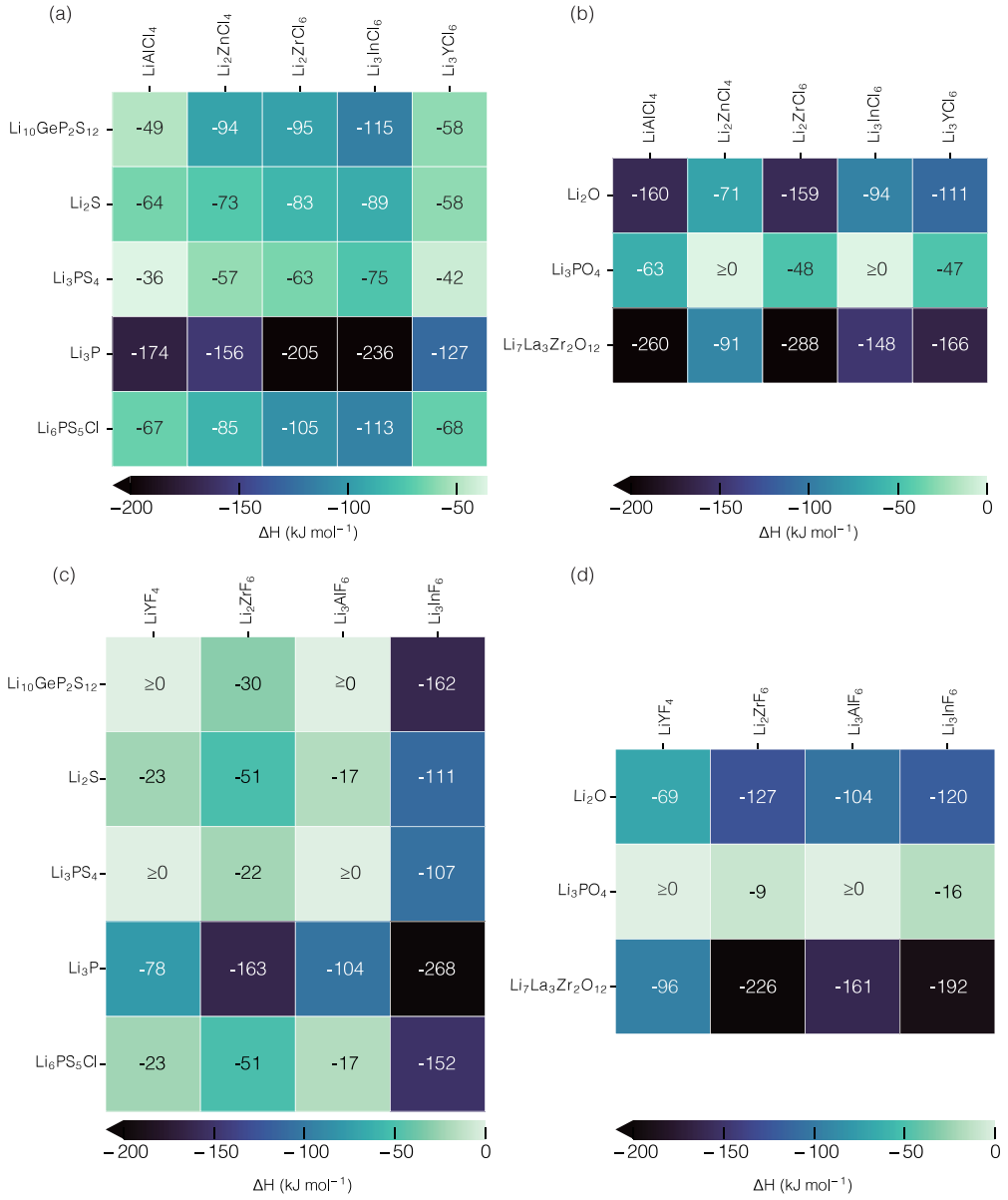

Figure 1. Chemical compatibility of anolytes and ternary chloride and fluoride catholytes (Li_iMX_j with X = F or Cl) in terms of computed ΔH (in kJ mol^{-1}). The anolytes are sulfides in panels (a) and (c) and are oxides in panels (b) and (d). The catholytes are chlorides in panels (a) and (b) and are fluorides in panels (c) and (d). ≥0 kJ mol^{-1} indicates the absence of reactivity. To simplify the presentation of the data, thiophosphate species such as, Li_3PS_4, Li_6PS_5Cl, and $Li_{10}GeP_2Ge(PS_6)_2$ are grouped with simpler sulfides, whereas Li_3PO_4 is grouped into oxides.

tored the magnitude of ΔH as the main descriptor to quantify the chemical stability of an interface.

$$\text{anolyte} + \text{catholyte} \xleftrightarrow{\Delta H} \sum_{i=1}^{n} \text{product}_i \tag{1}$$

Here, we report the reaction with the predicted lowest (most negative) ΔH from the analysis of the appropriate multi-component phase diagram. Additional reactions with more positive ΔH values are tabulated in the Supporting Information (SI).

As an example of the application of eq 1 to a real system, we consider the chemical reactivity of Li_3PS_4 as the anolyte and Li_3InCl_6 as the catholyte:

$$0.5\ Li_3PS_4\ (\text{anolyte}) + 0.5\ Li_3InCl_6\ (\text{catholyte}) \xrightarrow{\Delta H\ (-75\ \text{kJ mol}^{-1})} 0.5\ InPS_4 + 3\ LiCl \tag{2}$$

The reaction products resulting from eq 2 include the binary salt LiCl and the ternary thiophosphate $InPS_4$. Notably, the reaction presented in eq 2 is not a redox reaction; i.e., it does not involve a change in the oxidation states of the chemical species. It is instead a metathesis reaction. Further, the calculated reaction enthalpy of eq 2, $\Delta H = -75$ kJ mol^{-1}, is substantial. In practice, the value of ΔH is computed from the difference between the FEs of products and reactants as $\Delta H = 3 \times FE(LiCl) + 0.5 \times FE(InPS_4) - 0.5 \times FE(Li_3PS_4) - 0.5 \times FE(Li_3InCl_6)$. Here, FE is intended as the energy change to form a compound from its elemental constituents in their stable states under ambient conditions (298 K and 1 atm). For example, the formation energy of LiCl is the energy change

https://doi.org/10.1021/acsenergylett.4c02590
ACS Energy Lett. 2024, 9, 5935−5944

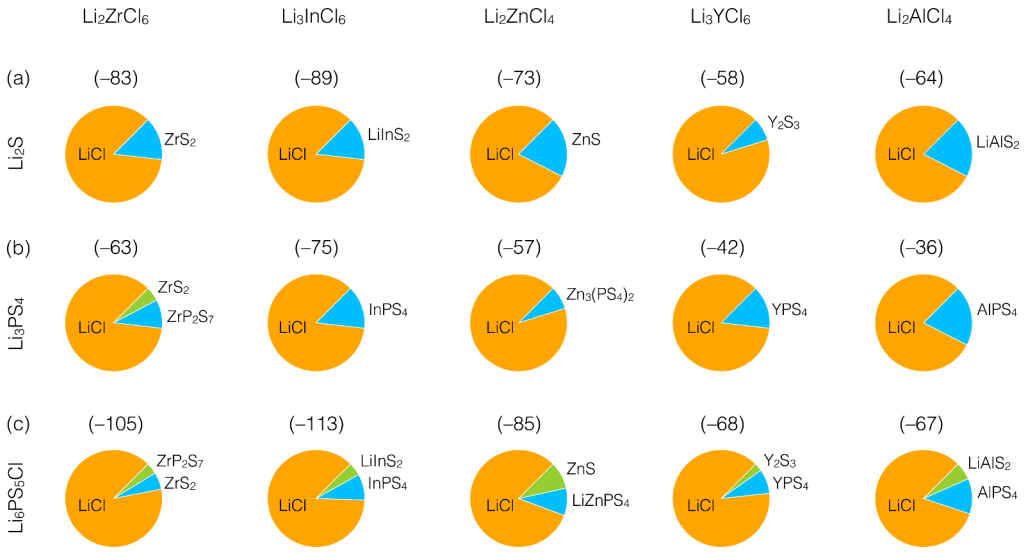

Figure 2. Predicted decomposition products when sulfur-containing anolytes react chemically with chloride catholytes. Reaction enthalpies are reported above each pie chart (in round brackets) in kJ mol^{-1}. The area of each slice is proportional to the mole fraction of the products formed based on the stoichiometry of the reaction, assuming that the reaction goes to completion.

associated with the reaction Li(s) + Cl_2(g) → LiCl(s). We note that the formation of quinary compounds based on Li−P−S−In−Cl, and with varying stoichiometries, were also considered. While we found no enthalpic gain in forming these quinary compounds upon mixing Li_3InCl_6 and Li_3PS_4 at room temperature (i.e., under typical battery operation conditions), such decomposition products may form at very high temperatures due to entropic stabilization.

We apply eq 1 to find all plausible decomposition reactions when mixing pairs of sulfide anolytes and chloride catholytes listed in Table 1. Figure 1a shows the heatmap for their computed DFT reaction enthalpies ΔH (in kJ mol^{-1}).

From Figure 1a, we observe that among the sulfur-containing compounds, the thiophosphate Li_3PS_4 shows the least reactivity with any of the ternary chlorides, with the Li_3PS_4/$LiAlCl_4$ interface featuring as the least reactive. Sulfide anolytes show the mildest reactivity when in contact with $LiAlCl_4$ and Li_3YCl_6 chloride catholytes. In contrast, sulfide anolytes appear to be the most reactive with Li_3InCl_6.

Given that Li_2S and Li_3P are common decomposition products of thiophosphates (e.g., Li_6PS_5Cl, Li_3PS_4, and $Li_{10}GeP_2S_{12}$) at low potentials, for example, when in contact with Li metal,[10,20,21] it is important to analyze the reactivity of these binary compounds (i.e., Li_2S and Li_3P) with the catholytes of interest. For Li_2S, the lowest and highest reaction enthalpies vary between −58 and −89 kJ mol^{-1} for Li_3YCl_6 and Li_3InCl_6, respectively. Among the anolytes studied here, we find Li_3P to be the most reactive; the highest reactivity is observed when Li_3P is paired with Li_3InCl_6 (−236 kJ mol^{-1}), and the least reactivity is observed when in contact with Li_3YCl_6 (−128 kJ mol^{-1}).

We next analyze the reactivity of the argyrodite electrolyte Li_6PS_5Cl with the chloride catholytes listed in Table 1. Li_6PS_5Cl has a high Li-ion conductivity in the range of 1−10 mS cm^{-1} at room temperature[50] and can be processed using a simple cold-pressing method, making it a viable SE for ASSBs.[2] Our results suggest that Li_6PS_5Cl reacts with all of the chloride catholytes studied here, with $\Delta H \leq -67$ kJ mol^{-1}. LiCl always features as a major (defined in terms of the number moles of LiCl per reaction) decomposition product for all pairs of Li_6PS_5Cl and chloride catholytes. This observation extends to all other anolytes containing sulfur species.

The most and least reactive pairs are shown in eqs 3 and 4:

$$0.6\,Li_3InCl_6 + 0.4\,Li_6PS_5Cl \xrightarrow{\Delta H\ (-113\ kJ\ mol^{-1})} 0.4\,InPS_4 + 0.2\,LiInS_2 + 4\,LiCl \quad (3)$$

$$0.6\,LiAlCl_4 + 0.4\,Li_6PS_5Cl \xrightarrow{\Delta H\ (-67\ kJ\ mol^{-1})} 0.2\,LiAlS_2 + 0.4\,AlPS_4 + 2.8\,LiCl \quad (4)$$

In addition to LiCl, reaction products include metal thiophosphates ($InPS_4$ and $AlPS_4$) and lithium metal sulfides ($LiInS_2$ and $LiAlS_2$). No change in the formal oxidation states of the elements occurs in eqs 3 and 4, classifying them as metathesis reactions.

Next, we extend this analysis to all bilayer separators formed between sulfides (including thiophosphates) and chloride catholytes and use pie charts to represent the distribution of reaction products, as shown in Figure 2. This figure only reports the reactions with the most negative values of ΔH. Pie charts illustrating the reaction of LGPS and Li_3P (as anolytes) with chloride catholytes are shown in Figure S1 of the SI.

The pie charts in Figure 2 reveal that LiCl always accounts for at least 75 mol % of the reaction products. Interestingly, similar reaction products are observed from the metathesis reactions between sulfides (except LGPS) and Li_3InCl_6, Li_3YCl_6, or $LiAlCl_4$, as shown in Table S1. This could be due to the common (3+) oxidation state of the transition metal in the chloride catholytes containing In, Y, or Al. In the case of LGPS, its reaction with Li_3InCl_6 is redox in nature, as revealed by the apparent changes in the oxidation states of the P (+5 in LGPS to +4 in $In_2(PS_3)_3$) and S (−2 in LGPS to −1 in P_2S_7) species.

We now consider the chemical compatibility of oxide anolytes with the chloride catholytes listed in Table 1. We include Li_2O in our list of oxides, as it is a common decomposition product of many oxide SEs (e.g., LLZO and LiPON) when placed in contact with Li metal.[11,51] The heatmap of Figure 1b shows the predicted reaction enthalpies when these two material classes react. Among the oxygen-containing solid electrolytes, Li_3PO_4 is the least reactive, and

https://doi.org/10.1021/acsenergylett.4c02590
ACS Energy Lett. 2024, 9, 5935−5944

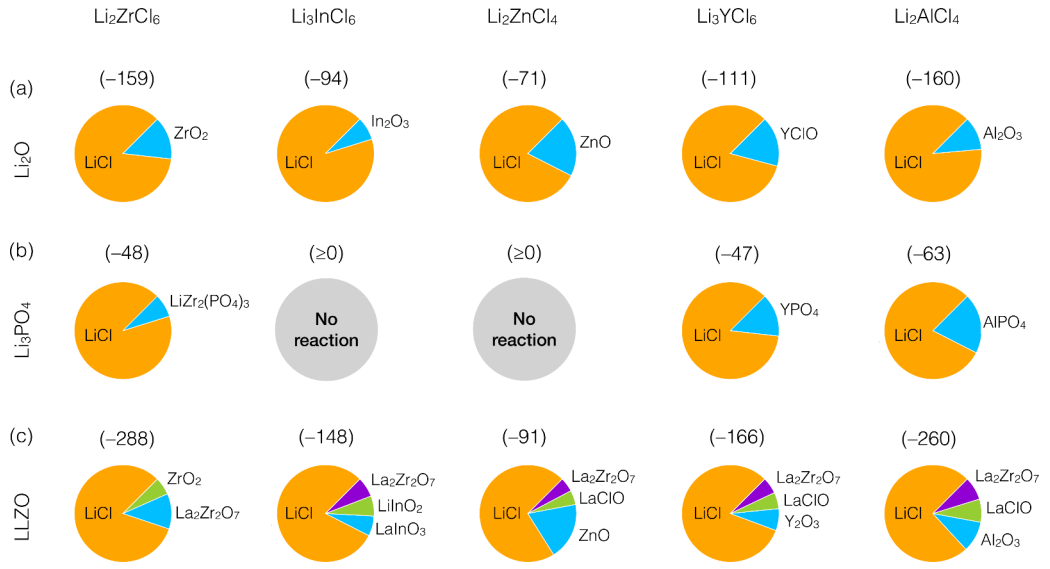

Figure 3. Predicted decomposition products when oxygen-containing anolytes react chemically with chloride catholytes. Reaction enthalpies are reported above each pie chart (in round brackets) in kJ mol^{-1}.

$Li_7La_3Zr_2O_{12}$ (LLZO) is the most reactive with the ternary chlorides. Oxide anolytes and Li_3PO_4 show the least reactivity with Li_2ZnCl_4, while they appear to be the most reactive with $LiAlCl_4$ and Li_2ZrCl_6.

We now analyze the reactivity of LLZO with different chlorides, as LLZO is the most widely studied oxide SE. Our results suggest that LLZO is highly reactive with all of the chloride catholytes investigated here, and LiCl consistently forms as a major decomposition product. This observation extends to all other oxide anolytes and Li_3PO_4 studied here. Equations 5 and 6 highlight the most and least reactive bilayer combinations with LLZO as the anolyte layer.

$$0.3636\ Li_7La_3Zr_2O_{12} + 0.6364\ Li_2ZrCl_6 \xrightarrow{\Delta H\ (-288\ kJ\ mol^{-1})} 0.5455\ La_2Zr_2O_7 + 0.2727\ ZrO_2 + 3.818\ LiCl \quad (5)$$

$$0.2\ Li_7La_3Zr_2O_{12} + 0.8\ Li_2ZnCl_4 \xrightarrow{\Delta H\ (-91\ kJ\ mol^{-1})} 0.2\ La_2Zr_2O_7 + 0.8\ ZnO + 0.2\ LaClO + 3\ LiCl \quad (6)$$

In both reactions (eqs 5 and 6), LiCl appears as the primary decomposition product, while $La_2Zr_2O_7$ and metal oxides (ZrO_2 and ZnO) form as minor phases. Additionally, LaClO forms when LLZO reacts with Li_2ZnCl_4. Notably, LiCl, ZrO_2, and ZnO are all extremely stable binary compounds. There is no change in the formal oxidation states of the elements in eqs 5 and 6, thereby classifying them as metathesis reactions.

Next, we extend this analysis to all bilayers formed between oxides and chloride catholytes and make use of pie charts to represent the distribution of reaction products (Figure 3). Unsurprisingly, LiCl is the primary product (in terms of mole fraction) formed. $La_2Zr_2O_7$ is another typical product of the reaction between LLZO and each of the chloride SEs considered here. All reaction products shown in Figure 3 arise from metathesis reactions rather than redox ones. The Li_3PO_4/Li_2ZnCl_4 and Li_3PO_4/Li_3InCl_6 pairings are predicted to be thermodynamically stable on account of their positive ΔH values and warrant further investigation. Hence, we will proceed to experimentally assess the chemical stability of one of these bilayer interfaces, namely Li_3PO_4/Li_3InCl_6, to test the validity of our predictions.

Details of the sample synthesis, handling, and characterization techniques are provided in Section S2 of the SI. The chemical stability of Li_3InCl_6 and Li_3PO_4 was tested experimentally by heat-treating a mixture of the pure compounds and analyzing the product. The two SE powder samples were mixed in a 1:1 molar ratio and then pressed into pellets to ensure good contact between the SEs during the subsequent heat treatment. One pellet was heat-treated at 300 °C for 24 h inside a fused quartz tube sealed under vacuum to accelerate the reaction between the two compounds; the resulting product is denoted "Mixed 300 °C". Another pellet was placed inside a fused quartz tube under vacuum and left at 25 °C for 24 h to mimic similar SE mixing conditions but without any heat treatment; the resulting product is referred to as "Mixed 25 °C". The Mixed pellets and pure (unmixed) compounds were subsequently analyzed at room temperature using a combination of X-ray diffraction (XRD), solid-state nuclear magnetic resonance (ssNMR), and X-ray photoelectron spectroscopy (XPS).

The XRD patterns obtained on the Mixed samples exhibit significantly broader reflections than those obtained on the pure powders (Figure S12). This broadening is at least in part due to a loss of crystallinity during the grinding step, as indicated by the broadening of the peaks observed in the XRD patterns obtained on each of the pristine (unreacted) compounds (Li_3InCl_6 and Li_3PO_4) after a similar grinding procedure (see Figure S14). Upon heat treatment of the Mixed 300 °C sample, the reflections corresponding to the Li_3InCl_6 and Li_3PO_4 phases sharpen, suggesting that some of the crystallinity is regained, but no new phases emerge (see Figure S12). The good stability of this electrolyte pairing is further confirmed by ^{6}Li and ^{31}P ssNMR. The spectra collected on the pure Li_3InCl_6 and Li_3PO_4 powder samples remain relatively unchanged after mixing at 25 °C and even after a 300 °C heat treatment, as shown in Figure 4a,b. A minor change in the occupancy of the P sites in Li_3PO_4 is evidenced by a change in the relative intensities of the signals in the Mixed ^{31}P spectra in Figure 4b. Regarding the ^{6}Li data in Figure 4a, the most intense signal in the two Mixed spectra, corresponding to Li species in the Li_3InCl_6 phase, is significantly broadened. This

https://doi.org/10.1021/acsenergylett.4c02590
ACS Energy Lett. 2024, 9, 5935−5944

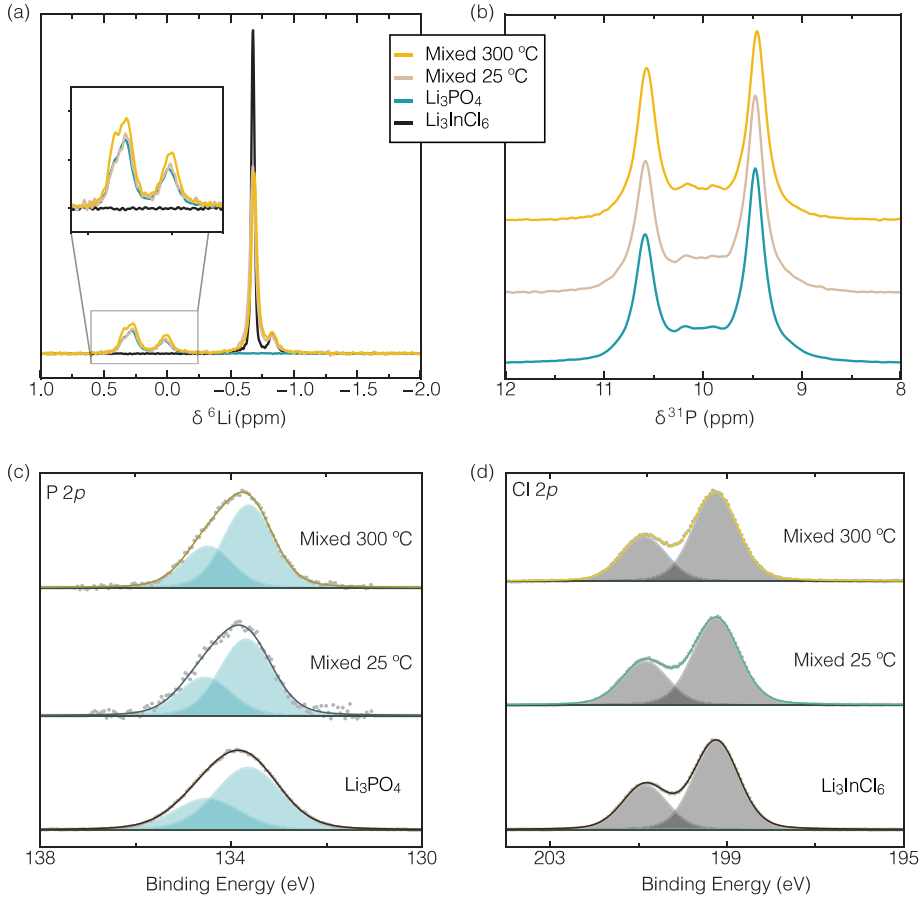

Figure 4. (a) ^{6}Li and (b) ^{31}P solid-state NMR spectra of Li_3InCl_6, Li_3PO_4, and the mixed and heat-treated samples. The spectra are scaled to maintain a constant total integrated intensity. All NMR data were collected using 30 kHz magic angle spinning at 18.8 T. High-resolution XPS spectra in the (c) P 2p and (d) Cl 2p regions for Li_3InCl_6, Li_3PO_4, and the mixed and heat-treated samples. Inset in (a) highlights possible changes in the ^{6}Li NMR spectra.

broadening is presumably due to an increase in the distribution of Li local environments (resulting in a narrow distribution of chemical shifts), in turn caused by positional disorder in the Li_3InCl_6 structure induced upon grinding the powders together. Structural disordering is also observed when Li_3InCl_6 is ground alone, as shown in Figure S14. The lack of significant change in the ^{6}Li and ^{31}P NMR spectra collected on the Mixed 25 °C and Mixed 300 °C samples confirms that the Li_3InCl_6 and Li_3PO_4 phases are stable after heat treatment, with no new Li- or P-containing phase (neither crystalline nor amorphous) formed. The P 2p and Cl 2p XPS spectra obtained on the pure compounds and the Mixed samples are presented in panels c and d of Figure 4, respectively. Figure S13 shows the Li 1s and In 3d XPS spectra for the unmixed and Mixed samples. Similar XPS peaks are observed in all samples considered. Taken together, the XRD, ssNMR, and XPS analyses confirm the excellent chemical compatibility of Li_3InCl_6 with Li_3PO_4 predicted with our computational framework.

Finally, we evaluated the chemical compatibility of sulfur- and oxygen-containing anolytes with the fluoride catholytes listed in Table 1. Figure 1c,d shows the heatmaps for their reaction enthalpies. It can be observed that Li_3PS_4 and Li_3PO_4 show the mildest reactivity, i.e., the best chemical compatibility, with fluoride catholytes. The sulfur- or oxygen-containing anolytes show the least reactivity with $LiYF_4$ and Li_3AlF_6. In contrast, the oxide anolytes appear to be the most reactive with Li_3InF_6. The reaction products are shown as pie charts in Figures S5−S7. We note that for the fluoride catholytes, the ΔH and the reaction products do not change significantly upon applying the second thermodynamic correction to the DFT results. Thus, this second correction is ignored. We find that bilayer interfaces with Li_3PS_4, LGPS, and Li_3PO_4 as anolytes and $LiYF_4$ and Li_3AlF_6 as catholytes provide positive ΔH. Thus, these six interfaces are predicted to be chemically compatible.

The experimental identification of viable bilayer interfaces and the experimental characterization of reactive (decomposing) bilayer interfaces in ASSBs remain as significant challenges due to their buried nature.[2,21] Computational materials science enables us to perform an extensive screening of potential material combinations of bilayer interfaces, thereby providing a bird's-eye view of this complex interfacial (and device) optimization problem. We analyzed the chemical compatibility of anolytes and catholytes forming a bilayer separator for ASSBs using a thermodynamic framework relying on first-principles calculations. Reaction enthalpies were used as descriptors to quantify the chemical compatibility of the bilayer separators. For one representative bilayer interface, Li_3PO_4/Li_3InCl_6, our computational results predicting their good chemical compatibility were confirmed experimentally.

While the preliminary step of computational screening using DFT calculations offers numerous advantages, these calculations are performed at 0 K, thus overlooking the entropic contributions to the chemical reactions. On the one hand,

https://doi.org/10.1021/acsenergylett.4c02590
ACS Energy Lett. 2024, 9, 5935−5944

considering entropic effects (vibrational and configurational) could change the predicted spontaneity of specific chemical reactions, particularly under moderate- to high-temperature conditions. On the other hand, this work demonstrates that the interfacial reaction products formed between anolytes and catholytes appear as "simple" binary or ternary compounds that are more ordered than the individual solid electrolyte materials, such as disordered ternary halides, quaternary argyrodite electrolytes, and LLZO in the case of oxides. This ordering will decrease the magnitude configurational entropy ΔS associated with most interfacial reactions. Negative values of ΔS will increase (make more positive) the associated Gibbs' free energy, decreasing the spontaneity of decomposition reactions. In this context, DFT-predicted thermodynamically stable interfaces with positive reaction enthalpies are expected to remain stable after considering the effect of the configurational entropy. In addition, predicted thermodynamically unstable interfaces with negative DFT reaction enthalpies may become stable after considering the impact of the configurational entropy.

DFT calculations predict the behavior of bilayer separators at thermodynamic equilibrium. However, the stability of the interface relies significantly on the kinetics of decomposition reactions, an aspect not considered by the theoretical models applied here. The formation of new thermodynamically stable interphases is linked to the likelihood of each ion diffusing through the materials near the interface. Focusing on the solid-state migration of cations, species with a small ionic radius (e.g., Li^+) and a small formal charge will migrate more efficiently than multivalent cations,[52−54] which may follow this qualitatively order $Zn^{2+} \gg Al^{3+}$, In^{3+}, Y^{3+}, $La^{3+} \gg Ge^{4+}$, $Zr^{4+} \gg P^{5+}$. These multivalent cations may diffuse sufficiently only if the temperature is high enough. In contrast, light and monovalent Li ions may reorganize efficiently at the temperature of the battery.

In the absence of chemical reactivity at the bilayer interface, a reduction in Li-ion transport in the interface may still be observed. The solid−solid interface formed between the anolyte and catholyte in the bilayer may need to accommodate substantial lattice mismatch imparted by the different chemistries of these materials.[55] Lattice mismatch may cause mechanical delamination and the creation of voids at the interface, which are detrimental to Li-ion transport.

We now compare the reaction products predicted herein to those reported previously when studying bilayer electrolyte cells. Starting with the thiophosphate/chloride pairings, Rosenbach et al.[12] studied the Li_6PS_5Cl/Li_3InCl_6 interface using time-of-flight secondary ion mass spectrometry and focused ion beam scanning electron microscopy. They detected the formation of an InS^- chemical feature, potentially linked to In_2S_3 or $LiInS_2$. Studying the same interface, Lee et al.[41] also identified In_2S_3, PS_4^{3-}, and P_2S_5 signatures by XPS. These reports indicate the instability of this particular bilayer.[12,41] The predictions for the Li_6PS_5Cl/Li_3InCl_6 interface in this work identified similar decomposition products (eq 3, Figure 2, Tables S1 and S3), such as $InPS_4$, $LiInS_2$, In_2S_3, and LiCl.

Koç et al.[38] reported the formation of LiCl as one of the decomposition products between Li_6PS_5Cl/Li_3InCl_6 and Li_3PS_4/Li_3InCl_6 interfaces and hypothesized that the chemical instability of these bilayer interfaces caused the observed degradation in battery performance. The electrochemical performance was improved by adding a nanometer-thick layer of Li_3PO_4 in between Li_6PS_5Cl (anolyte) and a composite positive electrode (Li_3InCl_6 with NMC622 as the active material and binders).[38] They thus inferred the stability of the Li_3PO_4/Li_3InCl_6 interface, which was verified here by our theoretical predictions (Figures 1b and 3) and further confirmed experimentally by using various characterization techniques. For bilayer separators comprising a chloride catholyte, our simulations shortlisted only two thermodynamically stable interfaces: Li_3PO_4/Li_2ZnCl_4, and Li_3PO_4/Li_3InCl_6.

Several observations can be made when comparing the chemical compatibilities of the anolytes with the fluoride and chloride catholytes investigated here. (i) Similar reactivity trends are observed for these two classes of catholytes. For example, Li_3PS_4 and Li_3PO_4 show the best chemical compatibility (out of all of the oxygen-, sulfur-, and phosphorus-containing anolytes considered here) with both chloride- and fluoride-based catholytes. In contrast, sulfur-containing anolytes show the highest reactivity with the Li_3InF_6 and Li_3InCl_6 catholytes. (ii) For those bilayer separators predicted to react, we also find that the reaction products from fluoride catholytes are similar to those from chloride catholytes. We have demonstrated that LiCl is a major product in decomposition reactions involving chloride-based catholytes. Similarly, LiF is a major decomposition product for all reacting fluoride-based bilayers (except for the thiophosphate LGPS) when pairing sulfur-containing anolytes with chloride- or fluoride-based catholytes, leading to a metathesis decomposition reactions.

Having established a parallel between the reactivity trends of chloride and fluoride catholytes, we compare their stability against sulfur- and oxygen-containing anolytes in terms of predicted ΔH values. Differences in ΔH values for fluoride and chloride catholytes are governed almost entirely by two main contributions: (i) on the product side of eq 1, the difference in formation energies (FEs) between LiCl and LiF, and (ii) on the reactant side, the difference in FEs between Li_iMCl_j and Li_iMF_j. The FEs of LiF and Li_iMF_j compounds are more negative than those of their chloride analogues, which is justified by the higher electronegativity of fluorine (~3.98 according to the Pauling scale) compared to that of chlorine (~3.16). Since LiF is a reaction product, its more negative FE makes the ΔH values of fluoride catholytes more negative (lower), that is to say, the reaction is more thermodynamically favorable, as compared to chlorides. In contrast, the more negative FE of Li_iMF_j increases their ΔH (more positive values) compared to their chloride analogues. The competing effects of the more negative FEs of LiF and Li_iMF_j regulate the propensity to decompose fluoride-based bilayer separators. We find that only Li_3InF_6-based bilayers have more negative ΔH values (making them less stable) as compared to Li_3InCl_6-based bilayers (Figure 1). All other fluoride-based bilayers considered here show more positive ΔH values than their chloride analogues, making them more stable.

This analysis suggests that considering the chemical compatibility of bilayer separators is vital when pairing SEs. However, the integrity of the bilayer separator is only preserved when the cell is operated within the electrochemical stability window (ESW) defined for bilayers by the reductive and oxidative potentials of the anolyte and catholyte, respectively. Outside the ESW, the SE may react and eventually decompose into other thermodynamically stable products.[11,51,56]

https://doi.org/10.1021/acsenergylett.4c02590
ACS Energy Lett. 2024, 9, 5935−5944

In the case of the Li_3PO_4/Li_3InCl_6 bilayer investigated here, Li_3PO_4 displays a reductive potential as low as ~0.7 vs Li/Li^+, whereas Li_3InCl_6 has a high oxidative potential of ~4.3 vs Li/Li^+ (see computed values in Figure S10). In strict mathematical terms, the union of the anolyte Li_3PO_4 reducing potential and the catholyte Li_3InCl_6 oxidative potential defines the ESW of the bilayer separator, which occurs in the 0.7−4.3 V vs Li/Li^+ range. Outside the 0.7−4.3 V voltage range, at least one SE is expected to decompose into simpler thermodynamically stable compounds at the corresponding potential. Excluding binary comopunds (Li_3P Li_2S, and Li_2O), none of the other anolyte materials investigated in this study appear stable at the potential of lithium metal (i.e., 0.0 V vs Li/Li^+). Recently, fully reduced materials, such as vacancy-rich $Li_9N_2Cl_3$[57] and antifluorite-like solid solutions between lithium binaries,[58] have been considered to solve this problem.

The development of viable all-solid-state batteries is limited by the lack of solid electrolytes that are simultaneously stable when in contact with both the high-voltage cathode and the low-voltage anode. Bilayer separators could potentially mitigate this issue, provided that the constituent materials are chemically compatible.

Using a robust thermodynamic framework powered by first-principles calculations, we investigated the chemical compatibility of 72 bilayer interfaces formed between halide catholytes and several types of anolytes containing oxygen, sulfur, and phosphorus species.

Among all of the anolytes studied, Li_3PS_4 (among sulfides) and Li_3PO_4 (among oxides) demonstrated the least reactivity with ternary halide catholytes. Our simulations identified a subset of bilayer separators with substantial chemical compatibility, making them potential candidates for use in ASSBs. In-depth experimental characterization of the Li_3PO_4/Li_3InCl_6 bilayer combination confirmed the innate chemical stability of this interface. This study underlines the importance of understanding the chemical stability of SE interfaces in bilayer ASSBs.

■ ASSOCIATED CONTENT

Supporting Information

The Supporting Information is available free of charge at https://pubs.acs.org/doi/10.1021/acsenergylett.4c02590.

Computational and experimental methodologies, approximations, and data analysis of the materials; computed reaction energies of anolytes and catholytes with multiple thermodynamic corrections; phase stability of ternary halides; experimental formation energies of binary and ternary compounds; computed electrochemical stability windows of bilayer separators; and X-ray diffractograms, XPS spectra, and ^6Li ssNMR spectra of Li_3InCl_6, Li_3PO_4, and their mixtures (PDF)

■ AUTHOR INFORMATION

Corresponding Authors

Raphaële J. Clément − *Materials Department and Materials Research Laboratory, University of California Santa Barbara, Santa Barbara, California 93106, United States;* orcid.org/0000-0002-3611-1162; Email: rclement@ucsb.edu

Pieremanuele Canepa − *Department of Electrical and Computer Engineering and Texas Center for Superconductivity, University of Houston, Houston, Texas 77204, United States;* orcid.org/0000-0002-5168-9253; Email: pcanepa@uh.edu

Authors

Abhishek A. Panchal − *Department of Electrical and Computer Engineering and Texas Center for Superconductivity, University of Houston, Houston, Texas 77204, United States;* orcid.org/0009-0004-4299-0302

Tyler N.T. Pennebaker − *Materials Department and Materials Research Laboratory, University of California Santa Barbara, Santa Barbara, California 93106, United States;* orcid.org/0000-0001-5119-0076

Elias Sebti − *Materials Department and Materials Research Laboratory, University of California Santa Barbara, Santa Barbara, California 93106, United States;* orcid.org/0000-0003-2678-3536

Yan Li − *Department of Materials Science and Engineering, National University of Singapore, Singapore 117575, Singapore*

Yuheng Li − *Department of Materials Science and Engineering, National University of Singapore, Singapore 117575, Singapore;* orcid.org/0000-0002-1865-1122

Complete contact information is available at: https://pubs.acs.org/10.1021/acsenergylett.4c02590

Notes

The authors declare no competing financial interest.

■ ACKNOWLEDGMENTS

P.C. acknowledges funding from the National Research Foundation under the NRFF12-2020-0012 program, Singapore. The computational work was performed on resources of the National Supercomputing Centre, Singapore (https://www.nscc.sg). We acknowledge the Robert A. Welch Foundation: L-E-001-19921203. This work used the shared facilities of the Materials Research Science and Engineering Center (MRSEC) at UC Santa Barbara: NSF DMR-2308708. The UC Santa Barbara MRSEC is a member of the Materials Research Facilities Network (https://www.mrfn.org/). This work was supported by LG Energy Solution—UC San Diego Frontier Research Laboratory via the Open Innovation program. The authors acknowledge using the Laboratory for Surface Characterization within the California NanoSystems Institute, supported by the University of California, Santa Barbara, and the University of California, Office of the President. This material is based upon work supported by the National Science Foundation Graduate Research Fellowship Program under Grant Nos. 1650114 and 2139319. Any opinions, findings, conclusions, or recommendations expressed in this material are those of the author(s) and do not necessarily reflect the views of the National Science Foundation.

■ REFERENCES

(1) Tian, Y.; Zeng, G.; Rutt, A.; Shi, T.; Kim, H.; Wang, J.; Koettgen, J.; Sun, Y.; Ouyang, B.; Chen, T.; Lun, Z.; Rong, Z.; Persson, K.; Ceder, G. Promises and Challenges of Next-Generation "Beyond Li-ion" Batteries for Electric Vehicles and Grid Decarbonization. *Chem. Rev.* **2021**, *121*, 1623−1669.

(2) Famprikis, T.; Canepa, P.; Dawson, J. A.; Islam, M. S.; Masquelier, C. Fundamentals of Inorganic Solid-State Electrolytes for Batteries. *Nat. Mater.* **2019**, *18*, 1278−1291.

(3) Janek, J.; Zeier, W. G. Challenges in Speeding up Solid-State Battery Development. *Nat. Energy* **2023**, *8*, 230−240.
(4) Manthiram, A.; Yu, X.; Wang, S. Lithium Battery Chemistries Enabled by Solid-State Electrolytes. *Nat. Rev. Mater.* **2017**, *2*, 16103.
(5) Janek, J.; Zeier, W. G. A Solid Future for Battery Development. *Nat. Energy* **2016**, *1*, 16141.
(6) Kato, Y.; Hori, S.; Saito, T.; Suzuki, K.; Hirayama, M.; Mitsui, A.; Yonemura, M.; Iba, H.; Kanno, R. High-Power All-Solid-State Batteries Using Sulfide Superionic Conductors. *Nat. Energy* **2016**, *1*, 16030.
(7) Park, K. H.; Bai, Q.; Kim, D. H.; Oh, D. Y.; Zhu, Y.; Mo, Y.; Jung, Y. S. Design Strategies, Practical Considerations, and New Solution Processes of Sulfide Solid Electrolytes for All-Solid-State Batteries. *Adv. Energy Mater.* **2018**, *8*, 1800035.
(8) Xiao, Y.; Wang, Y.; Bo, S.-H.; Kim, J. C.; Miara, L. J.; Ceder, G. Understanding Interface Stability in Solid-State Batteries. *Nat. Rev. Mater.* **2020**, *5*, 105−126.
(9) Kwak, H.; Wang, S.; Park, J.; Liu, Y.; Kim, K. T.; Choi, Y.; Mo, Y.; Jung, Y. S. Emerging Halide Superionic Conductors for All-Solid-State Batteries: Design, Synthesis, and Practical Applications. *ACS Energy Lett.* **2022**, *7*, 1776−1805.
(10) Richards, W. D.; Miara, L. J.; Wang, Y.; Kim, J. C.; Ceder, G. Interface Stability in Solid-State Batteries. *Chem. Mater.* **2016**, *28*, 266−273.
(11) Zhu, Y.; He, X.; Mo, Y. Origin of Outstanding Stability in the Lithium Solid Electrolyte Materials: Insights from Thermodynamic Analyses Based on First-Principles Calculations. *ACS Appl. Mater. Interfaces* **2015**, *7*, 23685−23693.
(12) Rosenbach, C.; Walther, F.; Ruhl, J.; Hartmann, M.; Hendriks, T. A.; Ohno, S.; Janek, J.; Zeier, W. G. Visualizing the Chemical Incompatibility of Halide and Sulfide-Based Electrolytes in Solid-State Batteries. *Adv. Energy Mater.* **2023**, *13*, 2203673.
(13) Allen, J.; Wolfenstine, J.; Rangasamy, E.; Sakamoto, J. Effect of substitution (Ta, Al, Ga) on the conductivity of $Li_7La_3Zr_2O_{12}$. *J. Power Sources* **2012**, *206*, 315−319.
(14) Li, X.; Liang, J.; Yang, X.; Adair, K. R.; Wang, C.; Zhao, F.; Sun, X. Progress and Perspectives on Halide Lithium Conductors for All-Solid-State Lithium Batteries. *Energy Environ. Sci.* **2020**, *13*, 1429−1461.
(15) Asano, T.; Sakai, A.; Ouchi, S.; Sakaida, M.; Miyazaki, A.; Hasegawa, S. Solid Halide Electrolytes with High Lithium-Ion Conductivity for Application in 4 V Class Bulk-Type All-Solid-State Batteries. *Adv. Mater.* **2018**, *30*, 1803075.
(16) Li, X.; et al. Air-Stable Li_3InCl_6 Electrolyte with High Voltage Compatibility for All-Solid-State Batteries. *Energy Environ. Sci.* **2019**, *12*, 2665−2671.
(17) Li, X.; Liang, J.; Chen, N.; Luo, J.; Adair, K. R.; Wang, C.; Banis, M. N.; Sham, T.-K.; Zhang, L.; Zhao, S.; Lu, S.; Huang, H.; Li, R.; Sun, X. Water-Mediated Synthesis of a Superionic Halide Solid Electrolyte. *Angew. Chem.* **2019**, *131*, 16579−16584.
(18) Sebti, E.; Evans, H. A.; Chen, H.; Richardson, P. M.; White, K. M.; Giovine, R.; Koirala, K. P.; Xu, Y.; Gonzalez-Correa, E.; Wang, C.; Brown, C. M.; Cheetham, A. K.; Canepa, P.; Clément, R. J. Stacking Faults Assist Lithium-Ion Conduction in a Halide-Based Superionic Conductor. *J. Am. Chem. Soc.* **2022**, *144*, 5795−5811.
(19) Riegger, L. M.; Schlem, R.; Sann, J.; Zeier, W. G.; Janek, J. Lithium-Metal Anode Instability of the Superionic Halide Solid Electrolytes and the Implications for Solid-State Batteries. *Angew. Chem., Int. Ed.* **2021**, *60*, 6718−6723.
(20) Wenzel, S.; Sedlmaier, S. J.; Dietrich, C.; Zeier, W. G.; Janek, J. Interfacial Reactivity and Interphase Growth of Argyrodite Solid Electrolytes at Lithium Metal Electrodes. *Solid State Ionics* **2018**, *318*, 102−112.
(21) Wang, J.; Panchal, A. A.; Sai Gautam, G.; Canepa, P. The Resistive Nature of Decomposing Interfaces of Solid Electrolytes with Alkali Metal Electrodes. *J. Mater. Chem. A* **2022**, *10*, 19732−19742.
(22) Krauskopf, T.; Richter, F. H.; Zeier, W. G.; Janek, J. Physicochemical Concepts of the Lithium Metal Anode in Solid-State Batteries. *Chem. Rev.* **2020**, *120*, 7745−7794.
(23) Kochetkov, I.; Zuo, T.-T.; Ruess, R.; Singh, B.; Zhou, L.; Kaup, K.; Janek, J.; Nazar, L. Different Interfacial Reactivity of Lithium Metal Chloride Electrolytes with High Voltage Cathodes Determines Solid-State Battery Performance. *Energy Environ. Sci.* **2022**, *15*, 3933−3944.
(24) Wang, C.; Liang, J.; Luo, J.; Liu, J.; Li, X.; Zhao, F.; Li, R.; Huang, H.; Zhao, S.; Zhang, L.; Wang, J.; Sun, X. A Universal Wet-Chemistry Synthesis of Solid-State Halide Electrolytes for All-Solid-State Lithium-Metal Batteries. *Sci. Adv.* **2021**, *7*, eabh1896.
(25) Zhou, L.; Zuo, T.-T.; Kwok, C. Y.; Kim, S. Y.; Assoud, A.; Zhang, Q.; Janek, J.; Nazar, L. F. High Areal Capacity, Long Cycle Life 4 V Ceramic All-Solid-State Li-ion Batteries Enabled by Chloride Solid Electrolytes. *Nat. Energy* **2022**, *7*, 83−93.
(26) Hendriks, T. A.; Lange, M. A.; Kiens, E. M.; Baeumer, C.; Zeier, W. G. Balancing Partial Ionic and Electronic Transport for Optimized Cathode Utilization of High-Voltage $LiMn_2O_4/Li_3InCl_6$ Solid-State Batteries. *Batteries & Supercaps* **2023**, *6*, e202200544.
(27) Kim, Y.; Juarez-Yescas, C.; Liao, D. W.; Jangid, M. K.; Joshi, P.; Yang, H.; Zahiri, B.; Braun, P. V.; Dasgupta, N. P. Thin Free-Standing Sulfide/Halide Bilayer Electrolytes for Solid-State Batteries Using Slurry Processing and Lamination. *ACS Energy Lett.* **2024**, *9*, 1353−1360.
(28) Wang, C.; Yu, R.; Duan, H.; Lu, Q.; Li, Q.; Adair, K. R.; Bao, D.; Liu, Y.; Yang, R.; Wang, J.; Zhao, S.; Huang, H.; Sun, X. Solvent-Free Approach for Interweaving Freestanding and Ultrathin Inorganic Solid Electrolyte Membranes. *ACS Energy Lett.* **2022**, *7*, 410−416.
(29) Jin, F.; Fadillah, L.; Nguyen, H. Q.; Sandvik, T. M.; Liu, Y.; García-Martín, A.; Salagre, E.; Michel, E. G.; Stoian, D.; Marshall, K.; Van Beek, W.; Redhammer, G.; Mehraj Ud Din, M.; Rettenwander, D. Elucidating the Impact of Li_3InCl_6-Coated $LiNi_{0.8}Co_{0.15}Al_{0.05}O_2$ on the Electro-Chemo-Mechanics of Li_6PS_5Cl-Based Solid-State Batteries. *Chem. Mater.* **2024**, *36*, 6017−6026.
(30) Ji, W.; Zheng, D.; Zhang, X.; Ding, T.; Qu, D. A Kinetically Stable Anode Interface for Li_3YCl_6-Based All-Solid-State Lithium Batteries. *J. Mater. Chem. A* **2021**, *9*, 15012−15018.
(31) Samanta, S.; Bera, S.; Biswas, R. K.; Mondal, S.; Mandal, L.; Banerjee, A. Ionocovalency of the Central Metal Halide Bond-Dependent Chemical Compatibility of Halide Solid Electrolytes with Li_6PS_5Cl. *ACS Energy Lett.* **2024**, *9*, 3683−3693.
(32) Luo, X.; Zhong, Y.; Wang, X.; Xia, X.; Gu, C.; Tu, J. Ionic Conductivity Enhancement of Li_2ZrCl_6 Halide Electrolytes via Mechanochemical Synthesis for All-Solid-State Lithium−Metal Batteries. *ACS Appl. Mater. Interfaces* **2022**, *14*, 49839−49846.
(33) Zhang, H.; Yu, Z.; Cheng, J.; Chen, H.; Huang, X.; Tian, B. Halide/Sulfide Composite Solid-State Electrolyte for Li-anode Based All-Solid-State Batteries. *Chin. Chem. Lett.* **2023**, *34*, 108228.
(34) Wang, K.; Ren, Q.; Gu, Z.; Duan, C.; Wang, J.; Zhu, F.; Fu, Y.; Hao, J.; Zhu, J.; He, L.; Wang, C.-W.; Lu, Y.; Ma, J.; Ma, C. A Cost-Effective and Humidity-Tolerant Chloride Solid Electrolyte for Lithium Batteries. *Nat. Commun.* **2021**, *12*, 4410.
(35) Luo, X.; Cai, D.; Wang, X.; Xia, X.; Gu, C.; Tu, J. A Novel Ethanol-Mediated Synthesis of Superionic Halide Electrolytes for High-Voltage All-Solid-State Lithium−Metal Batteries. *ACS Appl. Mater. Interfaces* **2022**, *14*, 29844−29855.
(36) Shi, J.; Yao, Z.; Xiang, J.; Cai, C.; Tu, F.; Zhang, Y.; Yao, W.; Jia, Q.; Zhou, Y.; Shen, S.; Yang, Y. High-Conductivity Li_2ZrCl_6 Electrolytes via an Optimized Two-Step Ball-Milling Method for All-Solid-State Lithium-Metal Batteries. *ACS Sustainable Chem. Eng.* **2024**, *12*, 2009−2017.
(37) Koç, T.; Marchini, F.; Rousse, G.; Dugas, R.; Tarascon, J.-M. In Search of the Best Solid Electrolyte-Layered Oxide Pairing for Assembling Practical All-Solid-State Batteries. *ACS Appl. Energy Mater.* **2021**, *4*, 13575−13585.
(38) Koç, T.; Hallot, M.; Quemin, E.; Hennequart, B.; Dugas, R.; Abakumov, A. M.; Lethien, C.; Tarascon, J.-M. Toward Optimization of the Chemical/Electrochemical Compatibility of Halide Solid Electrolytes in All-Solid-State Batteries. *ACS Energy Lett.* **2022**, *7*, 2979−2987.

https://doi.org/10.1021/acsenergylett.4c02590
ACS Energy Lett. 2024, 9, 5935−5944

(39) Kim, J. S.; Jung, S.; Kwak, H.; Han, Y.; Kim, S.; Lim, J.; Lee, Y. M.; Jung, Y. S. Synergistic Halide-Sulfide Hybrid Solid Electrolytes for Ni-rich Cathodes Design Guided by Digital Twin for All-Solid-State Li Batteries. *Energy Storage Mater.* **2023**, *55*, 193−204.
(40) Ye, Q.; Li, X.; Zhang, W.; Xia, Y.; He, X.; Huang, H.; Gan, Y.; Xia, X.; Zhang, J. Slurry-Coated $LiNi_{0.8}Co_{0.1}Mn_{0.1}O_2$−$Li_3InCl_6$ Composite Cathode with Enhanced Interfacial Stability for Sulfide-Based All-Solid-State Batteries. *ACS Appl. Mater. Interfaces* **2023**, *15*, 18878−18888.
(41) Lee, D.; Mesnier, A.; Manthiram, A. Crack-Free Single-Crystalline $LiNiO_2$ for High Energy Density All-Solid-State Batteries. *Adv. Energy Mater.* **2024**, *14*, 2303490.
(42) Luo, Q.; Liu, C.; Wei, C.; Wu, Z.; Wang, Y.; Li, L.; Jiang, Z.; Ming, L.; Yang, J.; Zhang, L.; et al. Deep insight of interfacial stability of $LiNi_{0.7}Co_{0.1}Mn_{0.2}O_2$-based all-solid-state battery with superior performances. *J. Power Sources* **2024**, *608*, 234616.
(43) Zhang, S.; Zhao, F.; Wang, S.; Liang, J.; Wang, J.; Wang, C.; Zhang, H.; Adair, K.; Li, W.; Li, M.; Duan, H.; Zhao, Y.; Yu, R.; Li, R.; Huang, H.; Zhang, L.; Zhao, S.; Lu, S.; Sham, T.-K.; Mo, Y.; Sun, X. Advanced High-Voltage All-Solid-State Li-Ion Batteries Enabled by a Dual-Halogen Solid Electrolyte. *Adv. Energy Mater.* **2021**, *11*, 2100836.
(44) Kim, S.; Lee, Y.; Kim, K.; Wood, B. C.; Han, S. S.; Yu, S. Fluorine-Substituted Lithium Chloride Solid Electrolytes for High-Voltage All-Solid-State Lithium-Ion Batteries. *ACS Energy Lett.* **2024**, *9*, 38−47.
(45) Wenzel, S.; Leichtweiss, T.; Krüger, D.; Sann, J.; Janek, J. Interphase formation on lithium solid electrolytes—An in situ approach to study interfacial reactions by photoelectron spectroscopy. *Solid State Ionics* **2015**, *278*, 98−105.
(46) Jain, A.; Hautier, G.; Ong, S. P.; Moore, C. J.; Fischer, C. C.; Persson, K. A.; Ceder, G. Formation Enthalpies by Mixing GGA and GGA+*U* Calculations. *Phys. Rev. B* **2011**, *84*, 045115.
(47) Kubaschewski, O.; Alcock, C. B. In *Metallurgical Thermochemistry*; Pergamon Press, 1979; p 267−323.
(48) Belsky, A.; Hellenbrandt, M.; Karen, V. L.; Luksch, P. New Developments in the Inorganic Crystal Structure Database (ICSD): Accessibility in Support of Materials Research and Design. *Acta Crystallogr., Sect. B: Struct. Sci.* **2002**, *58*, 364−369.
(49) Jain, A.; Ong, S. P.; Hautier, G.; Chen, W.; Richards, W. D.; Dacek, S.; Cholia, S.; Gunter, D.; Skinner, D.; Ceder, G.; Persson, K. A. Commentary: The Materials Project: A Materials Genome Approach to Accelerating Materials Innovation. *APL Mater.* **2013**, *1*, 011002.
(50) Deiseroth, H.-J.; Kong, S.-T.; Eckert, H.; Vannahme, J.; Reiner, C.; Zaiß, T.; Schlosser, M. Li_6PS_5X: A Class of Crystalline Li-Rich Solids With an Unusually High Li^+ Mobility. *Angew. Chem., Int. Ed.* **2008**, *47*, 755−758.
(51) Zhu, Y.; He, X.; Mo, Y. First Principles Study on Electrochemical and Chemical Stability of Solid Electrolyte−Electrode Interfaces in All-Solid-State Li-ion Batteries. *J. Mater. Chem. A* **2016**, *4*, 3253−3266.
(52) Rong, Z.; Malik, R.; Canepa, P.; Sai Gautam, G.; Liu, M.; Jain, A.; Persson, K.; Ceder, G. Materials Design Rules for Multivalent Ion Mobility in Intercalation Structures. *Chem. Mater.* **2015**, *27*, 6016−6021.
(53) Shewmon, P. In *Diffusion in Solids*, 2nd ed.; The Minerals, Metals & Materials Series; Springer International Publishing, Cham, Switzerland, 2016.
(54) Canepa, P.; Bo, S.-H.; Sai Gautam, G.; Key, B.; Richards, W. D.; Shi, T.; Tian, Y.; Wang, Y.; Li, J.; Ceder, G. High magnesium mobility in ternary spinel chalcogenides. *Nat. Commun.* **2017**, *8*, 1759.
(55) Xie, W.; Deng, Z.; Liu, Z.; Famprikis, T.; Butler, K. T.; Canepa, P. Effects of Grain Boundaries and Surfaces on Electronic and Mechanical Properties of Solid Electrolytes. *Adv. Energy Mater.* **2024**, *14*, 2304230.
(56) Wang, S.; Bai, Q.; Nolan, A. M.; Liu, Y.; Gong, S.; Sun, Q.; Mo, Y. Lithium Chlorides and Bromides as Promising Solid-State Chemistries for Fast Ion Conductors with Good Electrochemical Stability. *Angew. Chem., Int. Ed.* **2019**, *58*, 8039−8043.
(57) Li, W.; Li, M.; Chien, P.-H.; Wang, S.; Yu, C.; King, G.; Hu, Y.; Xiao, Q.; Shakouri, M.; Feng, R.; Fu, B.; Abdolvand, H.; Fraser, A.; Li, R.; Huang, Y.; Liu, J.; Mo, Y.; Sham, T.-K.; Sun, X. Lithium-compatible and air-stable vacancy-rich $Li_9N_2Cl_3$ for high−areal capacity, long-cycling all−solid-state lithium metal batteries. *Sci. Adv.* **2023**, *9*, eadh4626.
(58) Landgraf, V.; Tu, M.; Zhao, W.; Lavrinenko, A.; Cheng, Z.; Canals, J.; de Leeuw, J.; Ganapathy, S.; Vasileiadis, A.; Wagemaker, M.; Famprikis, T. Disorder-mediated ionic conductivity in irreducible solid electrolytes. *ChemRxiv* **2024**.

https://doi.org/10.1021/acsenergylett.4c02590
ACS Energy Lett. 2024, 9, 5935−5944